

## Inference of Granger causal time-dependent influences in noisy multivariate time series

Linda Sommerlade<sup>a,b,e,\*</sup>, Marco Thiel<sup>c</sup>, Bettina Platt<sup>d</sup>, Andrea Plano<sup>d</sup>, Gernot Riedel<sup>d</sup>, Celso Grebogi<sup>c,e</sup>, Jens Timmer<sup>a,b,e,f</sup>, Björn Schelter<sup>a,b,c,g</sup>

<sup>a</sup> Department of Physics, University of Freiburg, Hermann-Herder-Str. 3, 79104 Freiburg, Germany

<sup>b</sup> FDM, Freiburg Center for Data Analysis and Modeling, University of Freiburg, Eckerstr. 1, 79104 Freiburg, Germany

<sup>c</sup> Institute for Complex Systems and Mathematical Biology, SUPA, University of Aberdeen, Aberdeen AB24 3UE, UK

<sup>d</sup> Institute of Medical Sciences, University of Aberdeen, Foresterhill, Aberdeen AB25 2ZD, UK

<sup>e</sup> Freiburg Institute for Advanced Studies (FRIAS), University of Freiburg, Albertstr. 19, 79104 Freiburg, Germany

<sup>f</sup> Department of Clinical and Experimental Medicine, Linköping University, Sweden

<sup>g</sup> Division of Functional Brain Imaging (FBI), Department of Neurology, University Medical Center of Freiburg, Germany

### ARTICLE INFO

#### Article history:

Received 7 April 2011

Received in revised form 14 August 2011

Accepted 26 August 2011

#### Keywords:

Non-stationary causal influences  
Time-resolved partial directed coherence  
Vector autoregressive processes  
State space models  
Expectation–Maximization algorithm

### ABSTRACT

Inferring Granger-causal interactions between processes promises deeper insights into mechanisms underlying network phenomena, e.g. in the neurosciences where the level of connectivity in neural networks is of particular interest. Renormalized partial directed coherence has been introduced as a means to investigate Granger causality in such multivariate systems. A major challenge in estimating respective coherences is a reliable parameter estimation of vector autoregressive processes. We discuss two shortcomings typical in relevant applications, i.e. non-stationarity of the processes generating the time series and contamination with observational noise. To overcome both, we present a new approach by combining renormalized partial directed coherence with state space modeling. A numerical efficient way to perform both the estimation as well as the statistical inference will be presented.

© 2011 Elsevier B.V. All rights reserved.

### 1. Introduction

Several analysis techniques exist to determine relationships and causal influences in multivariate systems. Based on transfer entropy (Schreiber, 2000; Staniek and Lehnertz, 2008), recurrences in state space (Arnhold et al., 1999; Chicharro and Andrzejak, 2009; Romano et al., 2007), mutual information (Pompe et al., 1998; Paluš and Stefanovska, 2003; Paluš and Vejmelka, 2007; Vejmelka and Paluš, 2008; Frenzel and Pompe, 2007), phase dynamics (Rosenblum and Pikovsky, 2001; Rosenblum et al., 2002), coherence (Halliday and Rosenberg, 2000; Dahlhaus, 2000; Nolte et al., 2008), the Fokker Planck formalism (Prusseit and Lehnertz, 2008; Bahraminasab et al., 2009), or autoregressive processes (Dahlhaus and Eichler, 2003; Schack et al., 1995; Eichler, 2000; Korzeniewska et al., 1997; Kamiński et al., 1997; Kamiński and Blinowska, 1991; Arnold et al., 1998) they aim at detecting directed influences. Recently, partial directed coherence was introduced to

assess causal influences (Baccala and Sameshima, 2001) for example in neuroscience (Sameshima and Baccala, 1999; Nicolelis and Faselow, 2002). This frequency domain concept extends bivariate coherence analysis (Brockwell and Davis, 1993) and multivariate graphical models applying partial coherences (Dahlhaus, 2000; Brillinger, 1981). It has recently been generalized to renormalized partial directed coherence (Schelter et al., 2009), which allows the interpretation of the results also in terms of the strength of interaction.

In the neurosciences structural, functional and effective connectivity are distinguished (Horwitz, 2003). Here, we refer to functional connectivity unless otherwise stated. The functional connectivity of neural networks is usually estimated by classical methods like correlation and coherence based on raw data or power spectra approaches. All these methods do not give information about the direction of information flow. The use of Granger causality applied to electroencephalography (EEG) data is useful to identify the possible underlying functional network connectivity in order to gain information on the dynamics and connection strengths between different recording-sites.

Renormalized partial directed coherence is based on modeling time series by multivariate autoregressive processes. Commonly, the coefficients of such processes are estimated via the multivariate

\* Corresponding author at: FDM, Freiburg Center for Data Analysis and Modeling, University of Freiburg, Eckerstr. 1, 79104 Freiburg, Germany. Tel.: +49 761 203 7709; fax: +49 761 203 7700.

E-mail address: [linda.sommerlade@fdm.uni-freiburg.de](mailto:linda.sommerlade@fdm.uni-freiburg.de) (L. Sommerlade).

Yule Walker equations (Lütkepohl, 1993). Autoregressive models have the major drawback, that they are not able to cope with observational noise (Brockwell and Davis, 1993). Since neglecting the latter leads to a dramatic underestimation of the process coefficients, usually the order of the process is increased. This is not a sufficient solution to the challenge of observational noise (Timmer, 1998). The estimated coefficients of the autoregressive process are then Fourier transformed resulting in renormalized partial directed coherence, a quantity in the frequency domain replacing tests of statistical significance for the individual autoregressive coefficients.

The estimation algorithms assume stationarity and thus cannot deal with time-dependent autoregressive coefficients. Windowing the time series and analyzing the interaction structure in each window would result in an approximation of the results for non-stationary data, however, rapid changes in coefficients cannot be detected in this way. Actual estimation methods for time-dependent coefficients (Grenier, 1983; Kitagawa and Gersch, 1996; Wan and van der Merwe, 2000) are based on *a priori* information either about their functional relationship or at least about the smoothness of changes. A time-dependent implementation of autoregressive models and their corresponding parameter fitting algorithms is crucial for many applications such as transitions between sleep stages (Jyoti et al., 2010; Sunderam et al., 2007) or transitions into epileptic seizures (Gluckman et al., 2001; Sunderam et al., 2010).

Time-resolved Granger causality estimated from EEG data could for example be used as a mathematical tool to test hypothesis related to the interaction of brain areas. It could give important information and provide new insights into pathologies involving a fronto-temporal disconnection like schizophrenia (Lawrie et al., 2002) and confirm a possible mechanism providing a feasible biomarker for early disease detection or improved differential classification.

In task oriented and tactile exploratory movements an oscillatory activity in the beta frequency range (14–30 Hz) is observed in different part of the sensorimotor cortex (Brovelli et al., 2004). This observation suggests that the oscillations in the beta range could provide a mechanism that connects sensory and motor cortical areas during the tasks. Advancing this observation the Granger causality analysis allowing a narrow range spectral interpretation could reveal the directed influences between nodes in the sensorimotor brain networks.

The understanding of brain network dynamics based on EEG data may help to build a next level of logic built on the network structure combining other techniques that highlight structural connection like magnetic resonance imaging (MRI) (Seth and Edelman, 2007). Interestingly, the dynamic changes identified with Granger causality may depend on the context and behavioral situation of the measurement.

Some time-dependent methods (Winterhalder et al., 2005; Hemmelmann et al., 2009) do not specifically consider observational noise. To overcome the shortcomings introduced by observational noise and non-stationarity simultaneously, techniques that enable investigation of directional relationships on very short time scales from multiple realizations of short and transient noisy time series have been proposed (Andrzejak et al., 2006; Wagner et al., 2010; Martini et al., 2011). Using only single realizations, we combine state space modeling (Harvey, 1994; Shumway and Stoffer, 2000; Hamilton, 1994) with time-dependent autoregressive coefficients and renormalized partial directed coherence. Actual estimation techniques of time-dependent autoregressive coefficients in state space models are improved and enhanced for noisy and vector autoregressive processes. The presented estimator for the time-dependent autoregressive coefficients does not rely on any prior assumptions. This leads to a time resolving

analysis technique that detects causal influences between processes in multivariate systems contaminated with observational noise.

The paper is structured as follows: first, Section 2 summarizes renormalized partial directed coherence. Aspects of inadequate current estimators are discussed in Section 3. Time-dependent state space modeling and a parameter estimation technique able to cope with non-stationarity and observational noise are presented in Section 4. Examples of the combination of renormalized partial directed coherence and state space modeling are illustrated in Section 5, followed by an application to EEG data during sleep transitions recorded in mice in Section 6.

## 2. Renormalized partial directed coherence

Baccala and Sameshima et al. (Baccala and Sameshima, 2001, 1998; Baccala et al., 1998; Sameshima and Baccala, 1999) introduced partial directed coherence to examine causal influences in multivariate systems. This frequency domain measure was refined to allow to draw conclusions about the strength of interactions by renormalization (Schelter et al., 2009). In order to estimate renormalized partial directed coherence, a vector autoregressive process is fitted to the multivariate time series. Therefore, an  $n$ -dimensional vector autoregressive model of order  $p$  (VAR[ $p$ ])

$$\bar{\mathbf{x}}(t) = \sum_{r=1}^p \mathbf{a}_r \bar{\mathbf{x}}(t-r) + \bar{\boldsymbol{\varepsilon}}_x(t) \quad \bar{\boldsymbol{\varepsilon}}_x(t) \sim \mathcal{N}(\bar{\mathbf{0}} | \boldsymbol{\Sigma}) \quad (1)$$

is considered, where  $\bar{\boldsymbol{\varepsilon}}_x$  denotes independent Gaussian white noise with covariance matrix  $\boldsymbol{\Sigma}$  and  $\mathbf{a}_r$  the coefficient matrices of the VAR. A single component of such a vector autoregressive process can be interpreted in physical terms as a combination of relaxators and damped oscillators (Honerkamp, 1993).

The spectral matrix of a VAR process is given by Brockwell and Davis (1993)

$$\mathbf{S}(\omega) = \mathbf{H}(\omega) \boldsymbol{\Sigma} \mathbf{H}^H(\omega), \quad (2)$$

where the superscript  $(\cdot)^H$  denotes the Hermitian transpose. The transfer matrix  $\mathbf{H}(\omega)$  is defined as

$$\mathbf{H}(\omega) = [\mathbf{I} - \mathbf{A}(\omega)]^{-1} = [\bar{\mathbf{A}}(\omega)]^{-1}, \quad (3)$$

where  $\mathbf{I}$  is the  $n$ -dimensional identity matrix and  $\mathbf{A}(\omega)$  is given by the Fourier transform of the coefficients

$$\mathbf{A}_{kj}(\omega) = \sum_{r=1}^p \mathbf{a}_{r,kj} e^{-i\omega r}. \quad (4)$$

Consider the two-dimensional vector

$$\mathbf{X}_{kj}(\omega) = \begin{pmatrix} \text{Re}(\bar{\mathbf{A}}_{kj}(\omega)) \\ \text{Im}(\bar{\mathbf{A}}_{kj}(\omega)) \end{pmatrix} \quad (5)$$

with  $\mathbf{X}_{kj}(\omega) \mathbf{X}_{kj}(\omega) = |\bar{\mathbf{A}}_{kj}(\omega)|^2$ . The corresponding estimator  $\hat{\mathbf{X}}_{kj}(\omega)$  with  $\hat{\mathbf{A}}_{kj}(\omega)$  substituted for  $\mathbf{A}_{kj}(\omega)$  is asymptotically normally distributed with mean  $\mathbf{X}_{kj}(\omega)$  and covariance matrix  $\mathbf{V}_{kj}(\omega)/N$  (Schelter et al., 2009), where  $N$  is the number of data points and

$$\mathbf{V}_{kj}(\omega) = \sum_{l,m=1}^p \mathbf{R}_{jj}^{-1}(l,m) \boldsymbol{\Sigma}_{kk} \begin{pmatrix} \cos(l\omega) \cos(m\omega) & \cos(l\omega) \sin(m\omega) \\ \sin(l\omega) \cos(m\omega) & \sin(l\omega) \sin(m\omega) \end{pmatrix} \quad (6)$$

with  $\mathbf{R}$  the covariance matrix of the VAR process. This leads to the renormalized partial directed coherence

$$\lambda_{kj}(\omega) = \mathbf{X}_{kj}(\omega) \mathbf{V}_{kj}^{-1}(\omega) \mathbf{X}_{kj}(\omega). \quad (7)$$

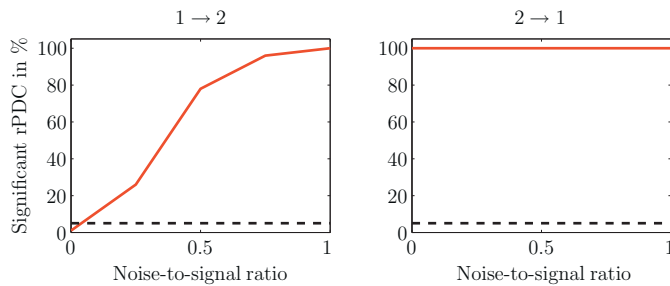


**Fig. 1.** Significant renormalized partial directed coherences in % of the 100 realizations for different amounts of observational noise. Renormalized partial directed coherence was estimated using a model order of  $p=10$ . Significance was evaluated at the oscillation frequencies of approximately 0.12 Hz and 0.05 Hz respectively.

If  $\lambda_{kj}(\omega) = 0$ , a Granger-causal linear influence from  $x_j$  to  $x_k$  taking all other processes into account can be rejected at frequency  $\omega$ . The  $\alpha$ -significance level for  $\lambda_{kj}(\omega) = 0$  is given by  $\chi^2_{2,1-\alpha}/N$  (Schelter et al., 2009).

### 3. Two shortcomings: observational noise and non-stationarity

Reliable estimation of  $n$ -dimensional VAR[ $p$ ] coefficient matrices is the major task in estimating renormalized partial directed coherence. Since in many applications observational noise is unavoidable, parameter estimation techniques like algorithms based on generalized Yule–Walker equations might yield misleading results.

This so-called *error-in-variables-problem* is illustrated in the following by an autoregressive process of order one (Timmer, 1998). For the parameter  $a$  of an AR[1]-process

$$x(t) = ax(t-1) + \varepsilon(t) \quad \varepsilon \sim \mathcal{N}(0, 1) \quad (8)$$

an unbiased estimator can be obtained based on the autocovariance function

$$\hat{a} = \frac{E[x(t)x(t-1)]}{E[x(t)x(t)]} \quad (9)$$

with  $E[\cdot]$  denoting the expectation value. Contamination with Gaussian distributed observational noise  $\eta(t)$

$$y(t) = x(t) + \eta(t) \quad (10)$$

leads to an underestimation of the parameter

$$\hat{a} = \frac{E[y(t)y(t-1)]}{E[y(t)y(t)]} = a \left[ 1 + \frac{E[\eta^2(t)]}{E[x^2(t)]} \right]^{-1}. \quad (11)$$

This underestimation becomes worse with increasing noise-to-signal ratio  $E[\eta^2(t)]/E[x^2(t)]$ . In the case of a noise-to-signal ratio of one, the estimated parameter  $\hat{a}$  reaches only 50% of the true value  $a$ .

The underestimation of parameters and its effects on renormalized partial directed coherence are illustrated in Fig. 1 for a 2-dimensional VAR[2] process

$$\vec{x}(t) = \sum_{r=1}^2 \mathbf{a}_r \vec{x}(t-r) + \vec{\varepsilon}_x(t), \quad (12)$$

$$y_i(t) = x_i(t) + \sigma_i \eta_i(t) \quad i = 1, 2, \quad (13)$$

with

$$\mathbf{a}_1 = \begin{pmatrix} 1.3 & c \\ 0 & 1.7 \end{pmatrix}, \quad \mathbf{a}_2 = \begin{pmatrix} -0.8 & 0 \\ 0 & -0.8 \end{pmatrix}. \quad (14)$$

The coupling parameter  $c$  was set to  $c=0.3$  and noise-to-signal ratios of  $\text{NSR} = 0$  to  $\text{NSR} = 1$  in steps of 0.25 were simulated by choosing the standard deviation of the observational noise  $\sigma_i$  accordingly. We simulated 100 realizations of  $N = 5000$  data points and used a model order of  $p = 10$  for the estimation. Assuming the true model order is unknown, if it is chosen too low, false positive conclusions may be drawn (Sommerlade et al., 2009). Thus, we chose the model order higher than the true one. The choice of 10 aims at demonstrating that a too high order does not spoil the results. Since the VAR[2] processes used here correspond to driven damped oscillators with a frequency of approximately 0.12 Hz and 0.05 Hz respectively, the renormalized partial directed coherence was evaluated at these frequencies. In Fig. 1 the percentage of significant renormalized partial directed coherences is shown in dependence of different noise-to-signal ratios. The number of erroneously detected interactions increases with increasing observational noise, while the true coupling is correctly detected for all NSRs.

Furthermore, if the interaction between the processes is not constant in time, the renormalized partial directed coherence analysis is expected to fail in estimating the true interaction structure. The causal influence from process  $x_2$  to  $x_1$  is represented by the parameter  $c$  in our model (Eqs. (12)–(14)). We set  $\sigma_i = 0$  for  $i = \{1, 2\}$ , i.e. no observational noise, and simulated a time dependent interaction by setting

$$c = \begin{cases} 0 & \text{if } t \leq 2500 \\ 0.5 & \text{else} \end{cases}, \quad (15)$$

i.e. the influence from process  $x_2$  to  $x_1$  is present only in the second half of the simulation period. Again we simulated 100 realizations of  $N = 5000$  data points and used a model of order  $p = 10$  for our estimation. Since the parameters are estimated for the whole time series, the renormalized partial directed coherence could not detect this time-dependence of the parameter. The influence from process  $x_2$  to  $x_1$  evaluated at 0.05 Hz was detected in 100% of the simulated realizations, which is misleading since the coupling is only present in the second half of the simulation.

In most applications, there is no prior knowledge about the time-dependence of parameters. Additionally, observational noise is usually present. Therefore, a time-dependent estimation technique that accounts for observational noise is required.

### 4. State-space modeling of time-dependent VAR processes contaminated with observational noise

To determine the time-dependent renormalized partial directed coherence the parameter matrices  $\mathbf{a}_1(t), \dots, \mathbf{a}_p(t)$  of an  $n$ -dimensional time-dependent vector autoregressive (VAR) process

$$\vec{x}(t) = \sum_{r=1}^p \mathbf{a}_r(t) \vec{x}(t-r) + \vec{\varepsilon}_x(t) \quad \vec{\varepsilon}_x(t) \sim \mathcal{N}(\vec{0} | \Sigma) \quad (16)$$

have to be estimated for each time-step. Furthermore, the estimator of the parameter matrices must take the additive Gaussian observational noise  $\vec{\eta}(t)$  contaminating the VAR[ $p$ ] process  $\vec{x}(t)$

$$\vec{y}(t) = \vec{x}(t) + \vec{\eta}(t) \quad \vec{\eta}(t) \sim \mathcal{N}(\vec{0} | \mathbf{R}), \quad (17)$$

into account.

The linear state space model is a powerful tool to estimate processes contaminated with observational noise as well as time-dependent parameters (Harvey, 1994; Kitagawa and Gersch, 1996). In the following, we introduce the concept of the linear state space modeling first in general and second for a stationary VAR[ $p$ ] process contaminated with observational noise. Finally, we generalize this state space description of the VAR[ $p$ ] process to time-dependent parameters  $\mathbf{a}_1(t), \dots, \mathbf{a}_p(t)$ .

To include observational noise explicitly, the state space model representation (Shumway and Stoffer, 2000; Harvey, 1994)

$$\bar{u}(t) = \mathbf{A}\bar{u}(t-1) + \bar{\varepsilon}_u(t) \quad \bar{\varepsilon}_u(t) \sim \mathcal{N}(\bar{\mathbf{0}}|\mathbf{Q}_u) \quad (18)$$

$$\bar{y}(t) = \mathbf{C}_u\bar{u}(t) + \bar{\eta}(t) \quad \bar{\eta}(t) \sim \mathcal{N}(\bar{\mathbf{0}}|\mathbf{R}) \quad (19)$$

where  $\bar{u}(t)$  is the multivariate hidden process and  $\bar{y}(t)$  the observed process contaminated with Gaussian noise  $\bar{\eta}(t)$ , of a VAR[1] process is used, handling of higher orders is introduced below.

In linear state space models, the optimal estimators for the hidden process  $\bar{u}(t)$ , given certain observations  $\{\bar{y}(1), \dots, \bar{y}(s)\}$  and assuming knowledge about the true parameters, are the Kalman filter (Kalman, 1960; Kalman and Bucy, 1961) and smoother (Rauch et al., 1965; Ansley and Kohn, 1982). The Kalman filter yields the conditional expectation value  $\bar{u}(t|t) := E\{\bar{u}(t)|\bar{y}(1), \dots, \bar{y}(t)\}$  considering only observations up to time  $t$ . The Kalman smoother, also called fixed interval smoother, calculates the conditional expectation value of the hidden process  $\bar{u}(t|N) := E\{\bar{u}(t)|\bar{y}(1), \dots, \bar{y}(N)\}$  taking account of all observations. These two estimators need the true parameters, i.e. the matrices  $\mathbf{A}$ ,  $\mathbf{Q}_u$ ,  $\mathbf{C}$ ,  $\mathbf{R}$  determining the linear model (18) and (19) as input. Thus, they are not sufficient to estimate the model parameters. The Expectation–Maximization (EM) algorithm (Dempster et al., 1977) applied to linear Gaussian state space models (Shumway and Stoffer, 1982) presents an iterative algorithm for Maximum Likelihood parameter estimation based on the Kalman filter and smoother.

A stationary VAR process of order  $p$  and dimension  $n$  as introduced in Eq. (1) can be rewritten as a process of first order by augmenting its dimension. Therefore, all past information needed to predict  $\bar{x}(t)$  is collected in one single new  $n_u$ -dimensional vector

$$\bar{u}(t-1) = (\bar{x}^T(t-1), \bar{x}^T(t-2), \dots, \bar{x}^T(t-p))^T, \quad (20)$$

with dimension  $n_u = np$ . The model equation

$$\underbrace{\begin{pmatrix} \bar{x}(t) \\ \bar{x}(t-1) \\ \vdots \\ \bar{x}(t-p+1) \end{pmatrix}}_{\bar{u}(t)} = \underbrace{\begin{pmatrix} \mathbf{a}_1 & \mathbf{a}_2 & \dots & \mathbf{a}_p \\ \mathbf{I}_n & \mathbf{0}_n & \dots & \mathbf{0}_n \\ \vdots & \ddots & \ddots & \vdots \\ \mathbf{0}_n & \dots & \mathbf{I}_n & \mathbf{0}_n \end{pmatrix}}_{\mathbf{A}} \underbrace{\begin{pmatrix} \bar{x}(t-1) \\ \bar{x}(t-2) \\ \vdots \\ \bar{x}(t-p) \end{pmatrix}}_{\bar{u}(t-1)} + \underbrace{\begin{pmatrix} \bar{\varepsilon}_x(t) \\ \bar{\mathbf{0}} \\ \vdots \\ \bar{\mathbf{0}} \end{pmatrix}}_{\bar{\varepsilon}_u(t)} \quad (21)$$

with

$$\bar{\varepsilon}_u(t) \sim \mathcal{N}\left(\bar{\mathbf{0}} \left| \begin{pmatrix} \Sigma & \mathbf{0}_n & \dots & \mathbf{0}_n \\ \mathbf{0}_n & \mathbf{0}_n & \dots & \mathbf{0}_n \\ \vdots & \ddots & \ddots & \vdots \\ \mathbf{0}_n & \dots & \mathbf{0}_n & \mathbf{0}_n \end{pmatrix} \right.\right) \quad (22)$$

$\underbrace{\hspace{10em}}_{\mathcal{N}(\bar{\mathbf{0}}|\mathbf{Q}_u)}$

of the new vector  $\bar{u}(t)$  is an equivalent representation of the VAR[ $p$ ] process  $\bar{x}(t)$ . The matrices  $\mathbf{I}_n$  and  $\mathbf{0}_n$  denote the  $n \times n$  identity and the  $n \times n$  matrix of zeros. The new representation in Eq. (21) of the VAR[ $p$ ] process ensures a direct applicability of the linear state space model of Eq. (18).

The state space model divides the VAR process contaminated with observational noise into two equations. The first, the system Eq. (18), describes the VAR[ $p$ ] process. The second, the observation Eq. (19)

$$\bar{y}(t) = \underbrace{\begin{pmatrix} \mathbf{I}_n & \mathbf{0}_n & \dots & \mathbf{0}_n \end{pmatrix}}_{\mathbf{C}_u} \bar{u}(t) + \bar{\eta}(t) = \bar{x}(t) + \bar{\eta}(t), \quad (23)$$

describes the observation of the  $n$ -dimensional vector  $\bar{x}(t)$  of the VAR[ $p$ ] process with additive observational noise  $\bar{\eta}_t$  of dimension

$n$ . Finally, the EM algorithm for the linear state space model in combination with the Kalman filter or smoother estimates the  $n^2(p+2)$  entries of the matrices  $\{\mathbf{a}_1, \dots, \mathbf{a}_p, \Sigma, \mathbf{R}\}$  as well as the hidden trajectory  $\{\bar{x}(1), \dots, \bar{x}(N)\}$  using only the observations  $\{\bar{y}(1), \dots, \bar{y}(N)\}$  (Shumway and Stoffer, 1982).

#### 4.1. Time-dependent parameters by the dual Kalman filter

To include non-stationary dynamics, state space modeling

$$\bar{u}(t) = \mathbf{A}^{\bar{a}(t-1)}\bar{u}(t-1) + \bar{\varepsilon}_u(t) \quad (24)$$

$$\bar{y}(t) = \mathbf{C}_u\bar{u}(t) + \bar{\eta}(t) \quad (25)$$

has to be extended to include time-dependent parameters  $\mathbf{A}^{\bar{a}(t-1)}$  with  $\mathbf{A}^{\bar{a}(t-1)}$  the matrix

$$\mathbf{A}^{\bar{a}(t-1)} = \begin{pmatrix} \mathbf{a}_1(t-1) & \mathbf{a}_2(t-1) & \dots & \mathbf{a}_p(t-1) \\ \mathbf{I}_n & \mathbf{0}_n & \dots & \mathbf{0}_n \\ \vdots & \ddots & \ddots & \vdots \\ \mathbf{0}_n & \dots & \mathbf{I}_n & \mathbf{0}_n \end{pmatrix} \quad (26)$$

that consists of the entries of the vector of the  $n^2p$  time varying entries of the coefficient matrices  $\mathbf{a}_1(t), \dots, \mathbf{a}_p(t)$  of the VAR[ $p$ ] process.

To estimate time-dependent parameters  $\bar{a}(t)$  together with the hidden process  $\bar{u}(t)$  the dual Kalman filter has been proposed (Wan and Nelson, 1997). For an approach based on a joint state space and the unscented Kalman filter (Julier et al., 2000) the dimension increases rapidly with the process dimension and order of the autoregressive model. Thus, we consider the dual approach here. Therefore, a second state space model complementing the one presented in Eqs. (24) and (25)

$$\bar{a}(t) = \bar{a}(t-1) + \bar{\varepsilon}_a(t) \quad (27)$$

$$\bar{y}(t) = \mathbf{C}_a^{\bar{u}(t-1)}\bar{a}(t) + \bar{\varepsilon}_x(t) + \bar{\eta}(t), \quad (28)$$

whereby  $\mathbf{C}_a^{\bar{u}(t-1)}$  denotes the observation matrix that results from the knowledge of  $\bar{u}(t-1)$ , has been introduced, which models the time-dependent parameters  $\bar{a}(t)$  as a hidden process. The hidden parameters are observed through the concatenated observation – (25) and process – (24) equation, i.e. the observation matrix  $\mathbf{C}_a^{\bar{u}(t-1)}$  contains the hidden process vector  $\bar{u}(t-1)$  in such a way that  $\mathbf{C}_a^{\bar{u}(t-1)}\bar{a}(t)$  correspond to the first  $n$  components of  $\mathbf{A}^{\bar{a}(t)}\bar{u}(t-1)$ .

We emphasize that the apparently non-stationary equation

$$\bar{a}(t) = \bar{a}(t-1) + \bar{\varepsilon}_a(t) \quad (29)$$

for the parameter vector can be interpreted as a restriction of the difference  $\bar{a}(t) - \bar{a}(t-1)$ , which is the discrete counterpart of the first derivative, by independent Gaussian distributed noise  $\bar{\varepsilon}_a(t) \sim \mathcal{N}(\bar{\mathbf{0}}|\mathbf{Q}_a)$  with a diagonal covariance matrix  $\mathbf{Q}_a$  (Kitagawa and Gersch, 1996). The variance  $(\mathbf{Q}_a)_{ii}$  determines the amount the parameter  $a_i(t)$  is allowed to change within one time step and thus the smoothness of the entire parameter curve  $a_i(t)$ .

The dual Kalman filter is divided into one linear Kalman filter for the process state space (24) and (25) and another one for the parameter state space (27) and (28). The process Kalman filter calculates the optimal estimates  $\bar{u}(t|t)$  given the time-dependent parameters  $\bar{a}(t-1)$  based on all causal observations. The parameter Kalman filter computes the optimal estimates  $\bar{a}(t|t)$  given the process state vectors  $\bar{u}(t-1)$ . Thus, the process Kalman filter depends on the parameters and the parameter Kalman filter relies on the process state vectors. This cross-over dependence of the parameter and process state space is resolved by using the estimates of the parameters  $\bar{a}(t-1|t-1)$  in the process Kalman filter and vice versa the results

**Table 1**

The dual state space model for the coefficients and process vectors of a time-dependent VAR[ $p$ ] process contaminated with observational noise is presented. The Expectation–Maximization algorithm is shown for this dual state space. The improvements of the dual Kalman filter are highlighted in red. The model and Expectation–Maximization algorithm are presented for the process state space on the left and the parameter state space on the right.

Time-dependent VAR[ $p$ ] process contaminated with observational noise

Dual state space model

Process state space

$$\tilde{u}(t) = \mathbf{A}(t)\tilde{u}(t-1) + \tilde{\epsilon}_u(t)$$

$$\tilde{y}(t) = \mathbf{C}_u\tilde{u}(t) + \tilde{\eta}(t)$$

Process transition matrix

$$\mathbf{A}^{\tilde{u}(t-1)} = \begin{pmatrix} a_1(t-1) & \cdots & a_{np}(t-1) \\ \vdots & \ddots & \vdots \\ a_{(n-1)p+1}(t-1) & \cdots & a_{np}(t-1) \\ \mathbf{I}_{np-n} & \mathbf{0}_{(np-n) \times n} \\ \mathbf{A}(t) := \mathbf{A}^{\tilde{u}(t-1)} \end{pmatrix} = \begin{pmatrix} \mathbf{A}_0(t) \\ \mathbf{A}_1 \end{pmatrix}$$

Expectation step

Improved dual Kalman filter

Process Kalman filter for  $t = 1, \dots, N$

Process transition matrix

$$\mathbf{A}(t|t-1) = \mathbf{A}^{\tilde{u}(t-1|t-1)} = \begin{pmatrix} \mathbf{A}_0(t|t-1) \\ \mathbf{A}_1 \end{pmatrix}$$

Process prediction

$$\begin{aligned} \tilde{u}(t|t-1) &= \mathbf{A}(t|t-1)\tilde{u}(t-1|t-1), \\ \mathbf{P}^u(t|t-1) &= \mathbf{A}(t|t-1)\mathbf{P}^u(t-1|t-1)\mathbf{A}^T(t|t-1) + \mathbf{Q}_u \\ \mathbf{P}^x(t|t-1) &= \mathbf{P}^x(t-1|t-1) + \mathbf{C}_a(t|t-1)\mathbf{P}^a(t-1|t-1)\mathbf{C}_a^T(t|t-1) \\ \mathbf{P}^{yu}(t|t-1) &= \mathbf{C}_u\mathbf{P}^u(t|t-1)\mathbf{C}_u^T + \mathbf{R} \end{aligned}$$

Process update

$$\begin{aligned} \mathbf{K}_u(t) &= \mathbf{P}^u(t|t-1)\mathbf{C}_u^T(\mathbf{P}^{yu}(t|t-1))^{-1} \\ \tilde{u}(t|t) &= \tilde{u}(t|t-1) + \mathbf{K}_u(t)(\tilde{y}(t) - \mathbf{C}_u\tilde{u}(t|t-1)), \\ \mathbf{P}^u(t|t) &= (\mathbf{I}_{np} - \mathbf{K}_u(t)\mathbf{C}_u)\mathbf{P}^u(t|t-1). \end{aligned}$$

Dual smoothing filter

Process smoothing filter for  $t = N, \dots, 1$

$$\begin{aligned} \mathbf{B}_u(t-1) &= \mathbf{P}^u(t-1|t-1)\mathbf{A}^T(t|t-1)(\mathbf{P}^u(t|t-1))^{-1} \\ \tilde{u}(t-1|N) &= \tilde{u}(t-1|t-1) + \mathbf{B}_u(t-1)(\tilde{u}(t|N) - \tilde{u}(t-1|t-1)) \\ \mathbf{P}^u(t-1|N) &= \mathbf{P}^u(t-1|t-1) + \mathbf{B}_u(t-1) \cdot \\ &\quad (\mathbf{P}^u(t|N) - \mathbf{P}^u(t|t-1))\mathbf{B}_u^T(t-1) \end{aligned}$$

Maximization step

$$\begin{aligned} \mathbf{A}(t|N) &:= \mathbf{A}^{\tilde{u}(t-1|N)} \\ \mathbf{Q}_u^{(m+1)} &= \frac{1}{N} \sum_{t=1}^N \left\{ (\tilde{u}(t|N) - \mathbf{A}(t|N)\tilde{u}(t-1|N)) \cdot \right. \\ &\quad \left. (\tilde{u}(t|N) - \mathbf{A}(t|N)\tilde{u}(t-1|N))^T + \mathbf{P}^u(t|N) - \mathbf{A}(t|N)\mathbf{B}_u(t-1)\mathbf{P}^u(t|N) \right. \\ &\quad \left. - \mathbf{P}(t|N)\mathbf{B}_u^T(t-1)\mathbf{A}^T(t|N) + \mathbf{A}(t|N)\mathbf{P}^u(t-1|N)\mathbf{A}^T(t|N) \right\} \\ \mathbf{R}^{(m+1)} &= \frac{1}{N} \sum_{t=1}^N \left\{ (\tilde{y}(t) - \mathbf{C}_u\tilde{u}(t|N))(\tilde{y}(t) - \mathbf{C}_u\tilde{u}(t|N))^T \right. \\ &\quad \left. + \mathbf{C}_u\mathbf{P}^u(t|N)\mathbf{C}_u^T \right\}. \end{aligned}$$

Parameter state space

$$\tilde{a}(t) = \tilde{a}(t-1) + \tilde{\epsilon}_a(t)$$

$$\tilde{y}(t) = \mathbf{C}_a(t)\tilde{a}(t) + \tilde{\epsilon}_x(t) + \tilde{\eta}(t),$$

Parameter observation matrix

$$\mathbf{C}^{\tilde{u}(t-1)} = \begin{pmatrix} \tilde{u}^T(t-1) & \cdots & \tilde{0}_{np}^T \\ \vdots & \ddots & \vdots \\ \tilde{0}_{np}^T & \cdots & \tilde{u}^T(t-1) \end{pmatrix}$$

$$\mathbf{C}_a(t) := \mathbf{C}^{\tilde{u}(t-1)}$$

Parameter Kalman filter for  $t = 1, \dots, N$

Parameter observation matrix

$$\mathbf{C}_a(t|t-1) := \mathbf{C}^{\tilde{u}(t-1|t-1)}$$

Parameter prediction

$$\begin{aligned} \tilde{a}(t|t-1) &= \tilde{a}(t-1|t-1), \\ \mathbf{P}^a(t|t-1) &= \mathbf{P}^a(t-1|t-1) + \mathbf{Q}_a \\ \mathbf{P}^{ya}(t|t-1) &= \mathbf{C}_a(t|t-1)\mathbf{P}^a(t|t-1)\mathbf{C}_a^T(t|t-1) + \mathbf{Q}_u \\ &\quad + \mathbf{A}_0(t|t-1)\mathbf{P}^{yu}(t-1|t-1)\mathbf{A}_0^T(t|t-1) + \mathbf{R} \\ &= \mathbf{P}^{ya}(t|t-1) + \mathbf{C}_a(t|t-1)\mathbf{Q}_a\mathbf{C}_a^T(t|t-1) \end{aligned}$$

Parameter update

$$\begin{aligned} \mathbf{K}_a(t) &= \mathbf{P}^a(t|t-1)\mathbf{C}_a^T(t|t-1)(\mathbf{P}^{ya}(t|t-1))^{-1} \\ \tilde{a}(t|t) &= \tilde{a}(t|t-1) + \mathbf{K}_a(t)(\tilde{y}(t) - \mathbf{C}_a(t)\tilde{a}(t|t-1)), \\ \mathbf{P}^a(t|t) &= (\mathbf{I}_{n^2p} - \mathbf{K}_a(t)\mathbf{C}_a(t))\mathbf{P}^a(t|t-1). \end{aligned}$$

Parameter smoothing filter for  $t = N, \dots, 1$

$$\begin{aligned} \mathbf{B}_a(t-1) &= \mathbf{P}^a(t-1|t-1)(\mathbf{P}^a(t|t-1))^{-1} \\ \tilde{a}(t-1|N) &= \tilde{a}(t-1|t-1) + \mathbf{B}_a(t-1)(\tilde{a}(t|N) - \tilde{a}(t-1|t-1)) \\ \mathbf{P}^a(t-1|N) &= \mathbf{P}^a(t-1|t-1) + \mathbf{B}_a(t-1) \cdot \\ &\quad (\mathbf{P}^a(t|N) - \mathbf{P}^a(t|t-1))\mathbf{B}_a^T(t-1) \end{aligned}$$

$$\begin{aligned} \mathbf{Q}_a^{(m+1)} &= \frac{1}{N} \sum_{t=1}^N \left\{ (\tilde{a}(t|N) - \tilde{a}(t-1|N)) \cdot \right. \\ &\quad \left. (\tilde{a}(t|N) - \tilde{a}(t-1|N))^T + \mathbf{P}^a(t|N) - \mathbf{B}_a(t-1)\mathbf{P}^a(t|N) \right. \\ &\quad \left. - \mathbf{P}^a(t|N)\mathbf{B}_a^T(t-1) + \mathbf{P}^a(t-1|N) \right\} \end{aligned}$$

of the process Kalman filter  $\tilde{u}(t-1|t-1)$  to calculate the parameter estimates  $\tilde{a}(t|t)$  via the parameter Kalman filter.

#### 4.1.1. Improvement of the dual Kalman filter

The dual Kalman filter neglects the estimation error of  $\tilde{a}(t-1|t-1)$  in the process state space, Eqs. (24) and (25) (Wan and Nelson, 1997). Thus, the variance of the random variable  $u(t) = \mathbf{A}^{\tilde{u}(t-1)}\tilde{u}(t-1)$  given the observations  $\{\tilde{y}(1), \dots, \tilde{y}(t-1)\}$  calculated by

$$\begin{aligned} \mathbf{P}^u(t|t-1) &= \text{Var}(u(t) | \tilde{y}(1), \dots, \tilde{y}(t-1)) \\ &= \mathbf{A}^{\tilde{u}(t-1|t-1)}\mathbf{P}^u(t-1|t-1)\mathbf{A}^{\tilde{u}(t-1|t-1)} \end{aligned} \quad (30)$$

is underestimated. Instead of considering  $\tilde{a}(t-1)$  as exact, we treat it as a random variable and approximate  $u(t) = \mathbf{A}^{\tilde{u}(t-1)}\tilde{u}(t-1)$  by a

first order Taylor expansion. The first  $n$  components contain the actual VAR[ $p$ ] process vector  $\tilde{x}(t)$  defined by a nonlinear function  $f(\tilde{a}(t-1), \tilde{u}(t-1))$  of second order. This leads to a correction of the variance  $\mathbf{P}^x(t|t-1)$  of  $\tilde{x}(t)$  resulting in

$$\mathbf{P}_{t|t-1}^x = \mathcal{A}_{t|t-1}^0 \mathbf{P}_{t-1|t-1}^u (\mathcal{A}_{t|t-1}^0)^T + \mathbf{C}_{t,a} \mathbf{P}_{t-1|t-1}^a \mathbf{C}_{t,a}^T + \Sigma \quad (31)$$

with  $\mathbf{A}_{t|t-1}^0$  referring to the first  $n$  rows of transition matrix  $\mathbf{A}_{t|t-1}$  of the process state space. Details are given in Appendix A. In the same way, the parameter Kalman filter is improved. For the detailed improved dual Kalman filter equations please refer to Table 1.

The dual Kalman filter uses only causal information to calculate the estimates for  $\tilde{a}(t)$  and  $\tilde{u}(t)$ . The dual smoothing filter improves the estimates  $\tilde{a}(t|t)$  and  $\tilde{u}(t|t)$  of the dual Kalman filter using even

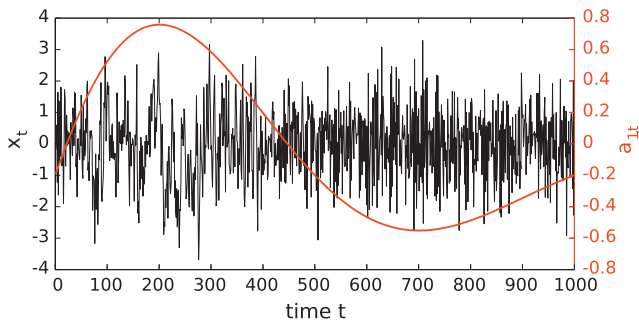


**Fig. 2.** One realization of a non-stationary AR[1] process is shown in black. The time-dependent AR coefficient  $a(t)$  is given in red. (For interpretation of the references to color in this figure legend, the reader is referred to the web version of the article.)

future observations. The dual smoothing filter equations to calculate  $\tilde{a}(t|N)\tilde{u}(t|N)$  are described in Table 1.

The usage of future observations however does not influence the estimation of causal relationships. The dual smoothing filter uses future observations to improve the estimation of the autoregressive coefficients. Thereby, the estimation is still based on Eqs. (24)–(28) and thus, only past values of  $\tilde{u}$  are allowed to influence the present value  $\tilde{u}(t)$ .

#### 4.1.2. Choosing the covariance $\mathbf{Q}_a$

Until now, we assumed that the variances  $\mathbf{Q}_a$ ,  $\Sigma$  and  $\mathbf{R}$  of the two state spaces were known. In the following, we demonstrate the importance of an adequate choice of the so-called smoothness prior  $\mathbf{Q}_a$  (Kitagawa and Gersch, 1996). To have a distinguishable notation, we are going to call the vector  $\tilde{a}(t)$  the parameters and the variances  $\mathbf{Q}_a$ ,  $\Sigma$  and  $\mathbf{R}$  hyper-parameters, although strictly speaking they are not hyper-parameters.

To investigate the results of the dual Kalman filter and dual smoothing filter, a one dimensional AR[1] process was simulated with a time varying parameter

$$a(t) = -0.2 + 1.5 \sin\left(\frac{2\pi t}{1000}\right) \exp\left(\frac{-2(t-1)}{999}\right). \quad (32)$$

The variance of the system noise  $\epsilon_x(t)$  was set to  $\Sigma = 1$ . In Fig. 2, the process variable  $x(t)$  and the time-depending AR coefficient  $a(t)$  are shown.

The observation of the time-dependent AR[1] process  $x_t$  is contaminated with observational noise  $\eta(t) \sim \mathcal{N}(0, R = 0.5)$ . Since the variance of the AR process depends on  $a(t)$  and thus on time, the noise-to-signal ratio lies between 0.2 and 0.5.

In Fig. 3, the time-dependent parameter of a one dimensional AR[1] process (Eq. (32)) is presented in black. The time-dependent parameter  $a(t)$  has been estimated by the dual smoothing filter. The process and observational noise variances have been set to the true values ( $\Sigma = 1$  and  $R = 0.5$ ) and the effect of using different parameter noise variances is demonstrated.

In Fig. 3(a), the parameter noise variance  $Q_a = 5 \times 10^{-2}$  is chosen too large and the estimator  $a(t|N)$  fluctuates around the true parameter curve. In Fig. 3(c), the  $Q_a = 5 \times 10^{-6}$  is very small and the Kalman smoother results cannot follow the true parameter values. In Fig. 3(b), the estimated parameters capture the true parameters with a parameter noise variance of  $Q_a = 5 \times 10^{-4}$  well. This example demonstrates that the parameter  $a(t)$  can only be estimated well if the hyper-parameters  $Q_a$ ,  $\Sigma$  and  $R$  are well known.

#### 4.2. Estimation of time-dependent parameters and stationary hyper-parameters by the EM algorithm

A Maximum Likelihood approach to estimate the hidden state vectors  $\{\tilde{a}(1), \dots, \tilde{a}(N), \tilde{u}(1), \dots, \tilde{u}(N)\}$  as well as the hyper-parameters  $\theta$  containing all unknown elements of  $\{\mathbf{Q}_a, \Sigma, \mathbf{R}\}$  is the Expectation–Maximization (EM) algorithm for linear state space models (Shumway and Stoffer, 1982). The algorithm uses in its expectation step the dual smoothing filter to calculate the estimates  $\tilde{u}(t|N), \tilde{a}(t|N)$  and their variances  $\mathbf{P}^u(t|N), \mathbf{P}^a(t|N)$  of the hidden processes  $\tilde{u}(t)$  and parameters  $\tilde{a}(t)$ . With the results of the expectation step the most likely hyper-parameters  $\hat{\theta}^{n+1}$  are calculated analytically in the maximization step, analog to the ordinary EM algorithm. Since the estimator  $\hat{\theta}^{n+1}$  of the hyper-parameters  $\theta$  depends on the results of the dual smoothing filter, which themselves depend on the hyper-parameters  $\theta^n$  used in the expectation step, this is a self-consistency problem. Therefore, the expectation and maximization step are iterated until it converges, which is checked by quantification of the parameter changes. The detailed EM algorithm for the two state spaces is resumed in Table 1.

To examine the results of the EM algorithm we apply it to the noise-contaminated time-dependent AR[1] process presented in Fig. 2. Thereby, we use two different kinds of expectation steps. First, the dual Kalman filter (Wan and Nelson, 1997) and second, the improved dual Kalman filter as introduced above is used. In Fig. 4, the convergence of the variances  $R$ ,  $\Sigma$ , and  $Q_a$  are shown for the two EM algorithms.

The Expectation–Maximization algorithms using the improved dual Kalman filter converges to the correct values of  $R$  and  $\Sigma$ , while

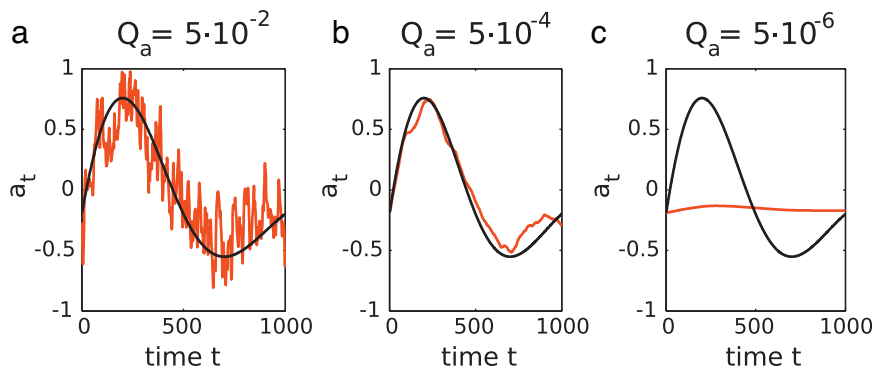


**Fig. 3.** The time-dependent parameter  $a(t)$  of an AR[1] process  $x(t) = a(t)x(t-1) + \epsilon_x(t)$  with  $\epsilon_x(t) \sim \mathcal{N}(0, 1)$  is presented in black. The time-dependent parameter is estimated by the dual smoothing filter. The system noise  $\Sigma = 1$ , the observational noise  $R = 0.5$  and three different parameter noise variances  $Q_a = 5 \times 10^{-2}, 5 \times 10^{-4}, 1 \times 10^{-6}$  are used for the dual smoothing filter. The results are shown in red in (a), (b) and (c) respectively. (For interpretation of the references to color in this figure legend, the reader is referred to the web version of the article.)

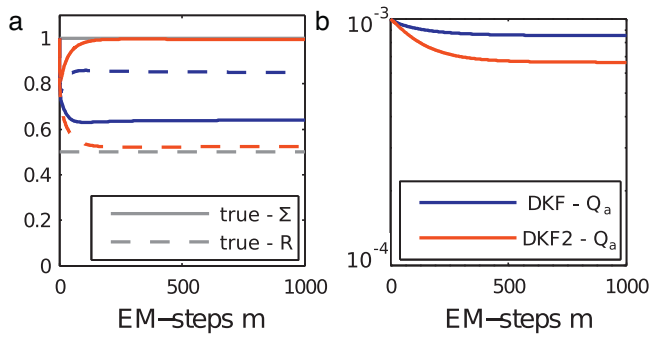


**Fig. 4.** The values of the hyper-parameters  $Q_a$ ,  $\Sigma$  and  $R$  are shown in dependence of the iterations of the Expectation–Maximization algorithm using the dual Kalman filter (DKF, blue) and the improved dual Kalman filter (DKF2, red) in the expectation step. In (a), the convergence of the variances of the process  $\Sigma$  (solid lines) and observational noise  $R$  (dashed lines) are compared to their true values. In (b), the development of the smoothness prior  $Q_a$  is shown. (For interpretation of the references to color in this figure legend, the reader is referred to the web version of the article.)

the results of the EM algorithm using the dual Kalman filter without improvements differ up to 70% from the original hyper-parameters (Fig. 4). Different estimated variances of the process and observational noise lead to different parameter estimates  $a(t|N)$  (not shown) and thus, to a different smoothness prior  $Q_a$  as seen in Fig. 4 b). The improved dual Kalman filter uses an improved estimation of the variances of all nonlinear contributions. Since the estimators for the variances of the observational and process noise  $\Sigma$ ,  $R$  depend strongly on the variance estimates of the process  $P^u(t|t)$ , parameters  $P^a(t|t)$  and observations  $P^y(t|t)$ , the improved dual Kalman filter is used in the Expectation–Maximization algorithm to obtain an unbiased estimator for  $\Sigma$  and  $R$ .

The presented estimation method for the parameters  $\bar{a}(t) = \{\mathbf{a}_1(t), \dots, \mathbf{a}_p(t)\}$  and hyper-parameters  $\bar{\theta} = \{\mathbf{R}, \Sigma, \mathbf{Q}_a\}$  of time-dependent VAR[ $p$ ] processes is compared to other techniques in (Grenier, 1983; Kitagawa and Gersch, 1996; Wan and van der Merwe, 2000) independent of prior knowledge. The computational effort of the EM algorithm is high for high dimensional, high-order VAR processes. The computing time for one Kalman filter iteration lies in the order  $\mathcal{O}(n_z^3)$ , where  $n_z$  is the dimension of the joint state space  $n_z = n_a + n_u = n^2 p + np$ . Since one iteration is required for each data point, the computing time of one expectation–maximization iteration is additionally scaled with the number of data points  $N$ . Increasing the dimension  $n$  of the system, the computing time

scales with  $n^6$ . Memory in the order of  $\mathcal{O}(N \cdot (n_a^2 + n_u^2))$  is demanded for the computation. Compared to a joint state space approach the dual approach already reduces the dimension of the state space since correlations between the process vector  $u$  and the coefficients  $a$  are discarded by separating two state spaces. We present several methods to additionally speed-up the algorithm and to reduce the dimension of the dual state space model in Appendix B.

## 5. Combination of renormalized partial directed coherence and state-space models

Since renormalized partial directed coherence is defined only by the  $p$  coefficient matrices of the VAR[ $p$ ] process underlying the time series, the determination of time-resolved renormalized partial directed coherence from noisy data corresponds to the estimation of a time-dependent VAR[ $p$ ] process from noisy data as proposed in the last section. Once the  $p$  VAR coefficient matrices are estimated  $\{\mathbf{a}_1(t), \dots, \mathbf{a}_p(t)\}$  renormalized partial directed coherence can be calculated for every time step  $t$  using Eq. (7).

As an example we use the 2-dimensional VAR[2] process Eq. (12) with coupling parameter  $c$  given in Eq. (15) and  $\sigma_i \neq 0$  respectively. The results for renormalized partial directed coherence in combination with the state-space models are shown in Figs. 5 and 6. For the estimation a model order of  $p = 10$  was used. Again the model order is chosen higher than the true model order since in an application the true process order is usually unknown. If the model order was chosen too low, spurious interaction might be detected. On the other hand if the model order is chosen far too high, true interactions might be discarded in the statistical fluctuations of rPDC. Thus, the model order should be chosen as high as necessary but as low as possible. Information criteria can guide the choice as suggested by Akaike (1974) and Schwarz (1978). Also a comparison of parametrically estimated spectra with their non-parametric counterparts is conceivable. Thus, the model order should be chosen as high as necessary but as low as possible. Concerning the time dependent coupling the influence from  $x_2$  to  $x_1$  was present only in the second half of the simulation. This interaction was correctly revealed by renormalized partial directed coherence in combination with the state-space models as shown in Fig. 5. Given a constant coupling  $c = 0.3$  the true interaction was revealed for different amounts of observational noise. Here, the noise-to-signal ratio was varied between NSR = 0 and NSR = 1 in steps of 0.25, exemplary results are depicted

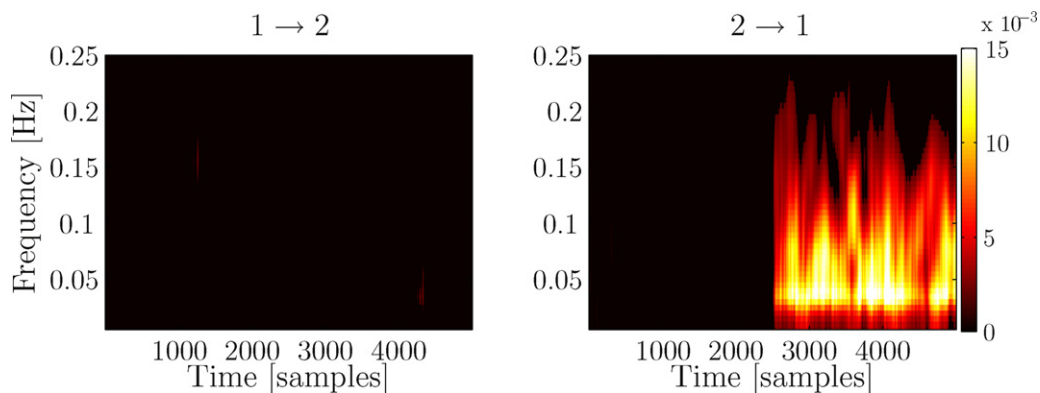


**Fig. 5.** Time-dependent renormalized partial directed coherence for 2-dimensional VAR[2] process with non-stationary coupling. On the left, renormalized partial directed coherence for the direction from  $x_1$  to  $x_2$  is shown. In the simulation the coupling from  $x_2$  to  $x_1$  is present only in the second half of the simulation, the results for this direction are shown on the right.

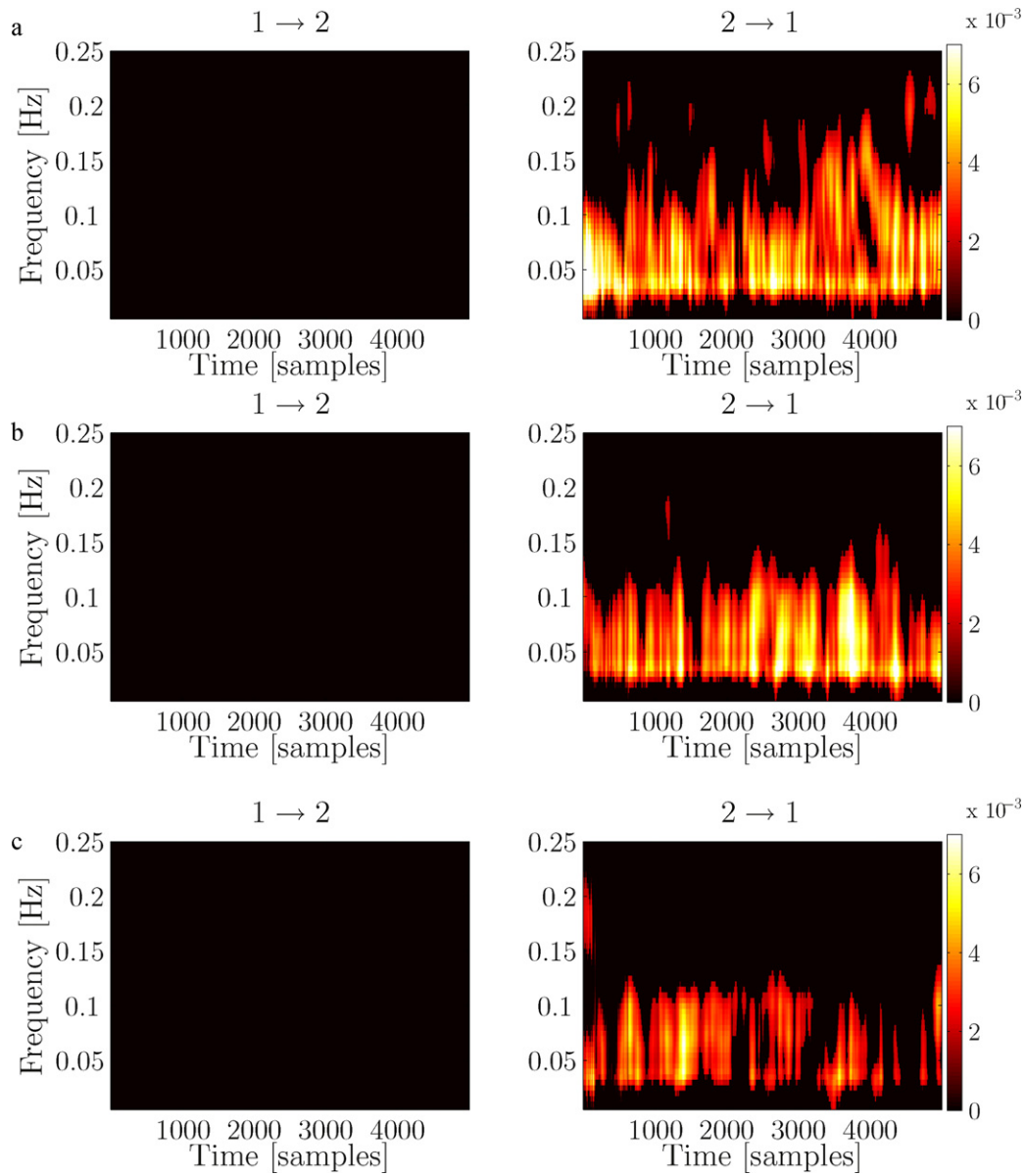


**Fig. 6.** Time-dependent renormalized partial directed coherence for 2-dimensional VAR[2] process with different amounts of observational noise. (a) No observational noise. (b) Noise-to-signal ratio of 0.5. (c) Noise-to-signal ratio of 1. On the left, renormalized partial directed coherence for the direction from  $x_1$  to  $x_2$  is shown. In the simulation only the coupling from  $x_2$  to  $x_1$  is present, the results for this direction are shown on the right.

in Fig. 6. Compared to renormalized partial directed coherence without state space modeling no false positive detections occurred here.

In order to illustrate the multivariate capability of the method presented here, we simulated a 4-dimensional VAR[2] process with  $N=5000$  data points and parameters

$$\mathbf{a}_1 = \begin{pmatrix} 1.3 & c_{12} & 0 & c_{14} \\ c_{21} & 1.6 & 0 & 0 \\ c_{31} & 0 & 1.5 & c_{34} \\ 0 & 0 & 0 & 1.7 \end{pmatrix} \quad (33)$$

$$\mathbf{a}_2 = \begin{pmatrix} -0.8 & 0 & 0 & 0 \\ 0 & -0.8 & 0 & 0 \\ 0 & 0 & -0.8 & 0 \\ 0 & 0 & 0 & -0.8 \end{pmatrix} \quad (34)$$

and

$$c_{31} = 0.5 \quad (35)$$

$$c_{12} = \begin{cases} 0 & \text{if } t \leq 3333 \\ 0.7 & \text{else} \end{cases} \quad (36)$$

$$c_{21} = \begin{cases} 0.7 & \text{if } t \leq 1666 \\ 0 & \text{else} \end{cases} \quad (37)$$

$$c_{34} = 0.8 \left( 1 - \frac{|t - 2500|}{2500} \right) \quad (38)$$

$$c_{14} = e^{-t/2500} \sin(0.005t) \quad (39)$$

This corresponds to the following interaction structure: the influence from  $x_1$  to  $x_3$  is constant for the whole simulation, the influence from  $x_1$  to  $x_2$  is present only in the first third of the simulation while the reverse direction ( $x_2$  to  $x_1$ ) is present in the last third. The influence from  $x_4$  to  $x_3$  starts with zero, is linearly increased

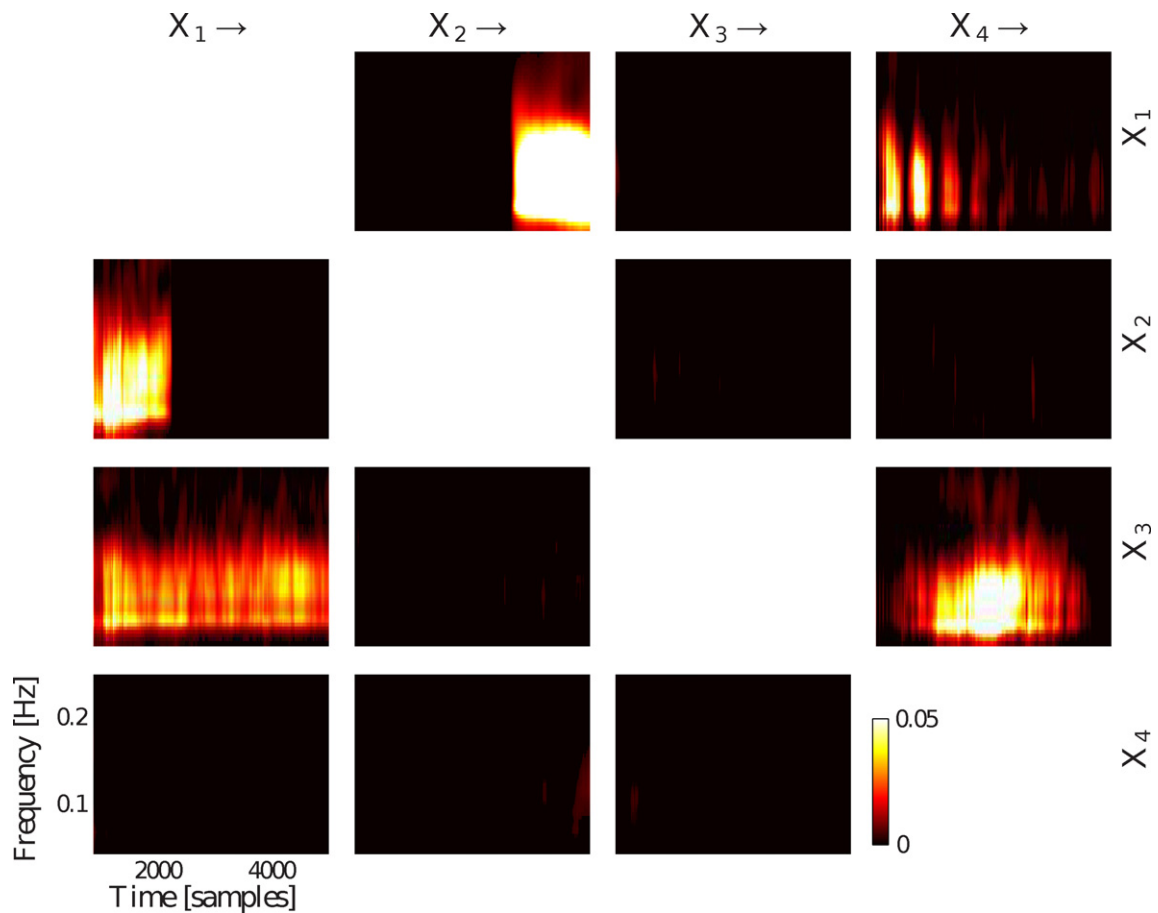


**Fig. 7.** Results of renormalized partial directed coherence analysis in combination with state space modeling for the 4-dimensional VAR[2] process (Eqs. (33)–(39)). Time resolved rPDC analysis with respect to frequency in Hz ( $y$ -axis) and time in samples ( $x$ -axis) is shown – direction of information flow is from column to row.

until the middle of the simulation and then linearly decreases to zero until the end of the simulation. The influence from  $x_4$  to  $x_1$  is modulated by a damped oscillation fading to zero in the end of the simulation. All other possible interactions are zero. The results using a model order of  $p = 10$  for this simulation are shown in Fig. 7. All simulated interactions are revealed correctly. Thus, the method presented here is capable of inferring the time dependent interaction structure in multivariate systems.

In order to test the multivariate capability of the method in the presence of noise, we reran the above simulation with 5% observational noise. As shown in Fig. 8 the simulated interactions were revealed correctly. We achieved satisfying results when testing for up to 25% observational noise (results not shown).

## 6. Application

To demonstrate the applicability of the proposed approach to a biological data set, we used EEG recordings from a mouse during a transition from slow-wave (NREM) to rapid eye movement (REM) sleep (Fig. 9). EEG recordings were obtained under freely-moving conditions with a wireless device (NeuroLogger, TSE Systems GmbH – Bad Homburg/Germany). The signal was pre-amplified (AC input range  $\pm 750 \mu\text{V}$ , unity gain buffer,  $500\times$  gain, band-pass filtered 1–70 Hz), sampled (199 Hz), analog-to-digital converted (ADC resolution 10 bits), and the data stored (capacity 256 MB) are handled by an on-board microcontroller. Gold screw electrodes were placed into the skull into bur holes at the following co-ordinates relative to Bregma above (i) medial pre-frontal cortex (PFx: AP +2 mm/close to midline); and (ii) parietal cortex and dorsal hippocampi (bilateral, AP +2 mm/1.5 mm lateral to midline).

Reference and ground electrodes were placed at neutral locations superficial to parietal and occipital cortex, respectively. For details of the recording technique, see (Jyoti et al., 2010).

The transition takes place after 16.7 s. The dataset was analyzed with time resolved renormalized partial directed coherence. A model order of  $p = 10$  was used as revealed by the Akaike information criterion (Akaike, 1974). The results (Fig. 9) illustrate a strong interaction between all brain regions particularly affecting frequencies close to 10 Hz, and coincident with the transition from slow-wave to REM sleep. Before the transition only short interactions are detected which are more irregular compared to the post-transition coherences.

In the prominent alpha range (i.e.  $\sim 10$  Hz), an influence from left hippocampus (IHC) to prefrontal cortex (PFx) occurred earliest in this example. The opposite direction (PFx to IHC) followed and strengthened towards the end of the recording. The onset of the influence from right hippocampus (rHC) to IHC was close to that of IHC to PFx. The strongest influence was found from rHC to IHC. Interestingly, interactions from IHC to rHC as well as from rHC to PFx were weaker, but increased towards the end of the recording.

Communication between hippocampus and prefrontal cortex areas play crucial roles in working memory and memory consolidation. Assessed in a robust way, the dynamics of how and when the communication occurs in different recording scales (EEG/LFP/single unit recording) is essential for the understanding of the behavioral relevance and may ultimately uncover bio-markers for neurodegenerative diseases. Indicators that enable the characterization of transitions and predict their onsets would be desirable, but cannot be achieved based on a single example. This will be subject to further investigations and involve transitions between other

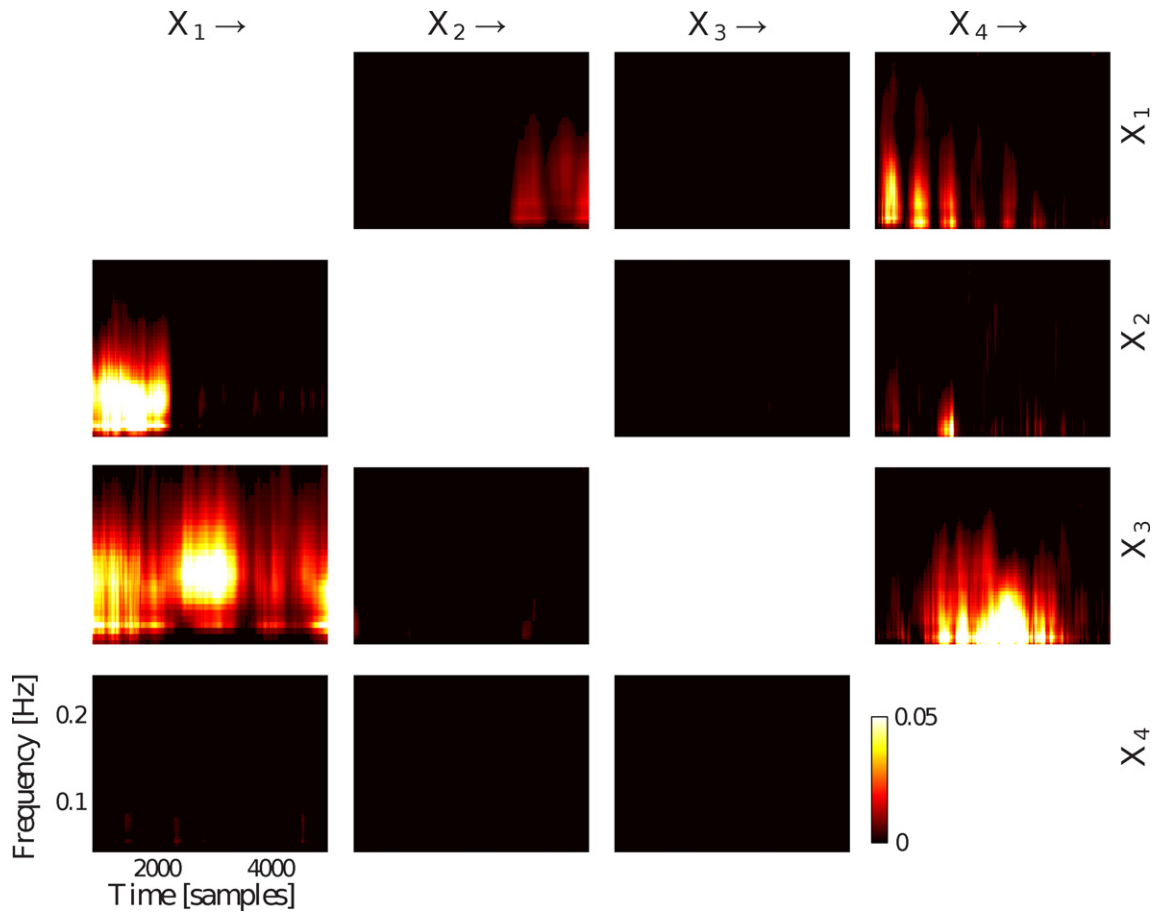


**Fig. 8.** Results of renormalized partial directed coherence analysis in combination with state space modeling for the 4-dimensional VAR[2] process (Eqs. (33)–(39)) with 5% observational noise. Time resolved rPDC analysis with respect to frequency in Hz (y-axis) and time in samples (x-axis) is shown – direction of information flow is from column to row.

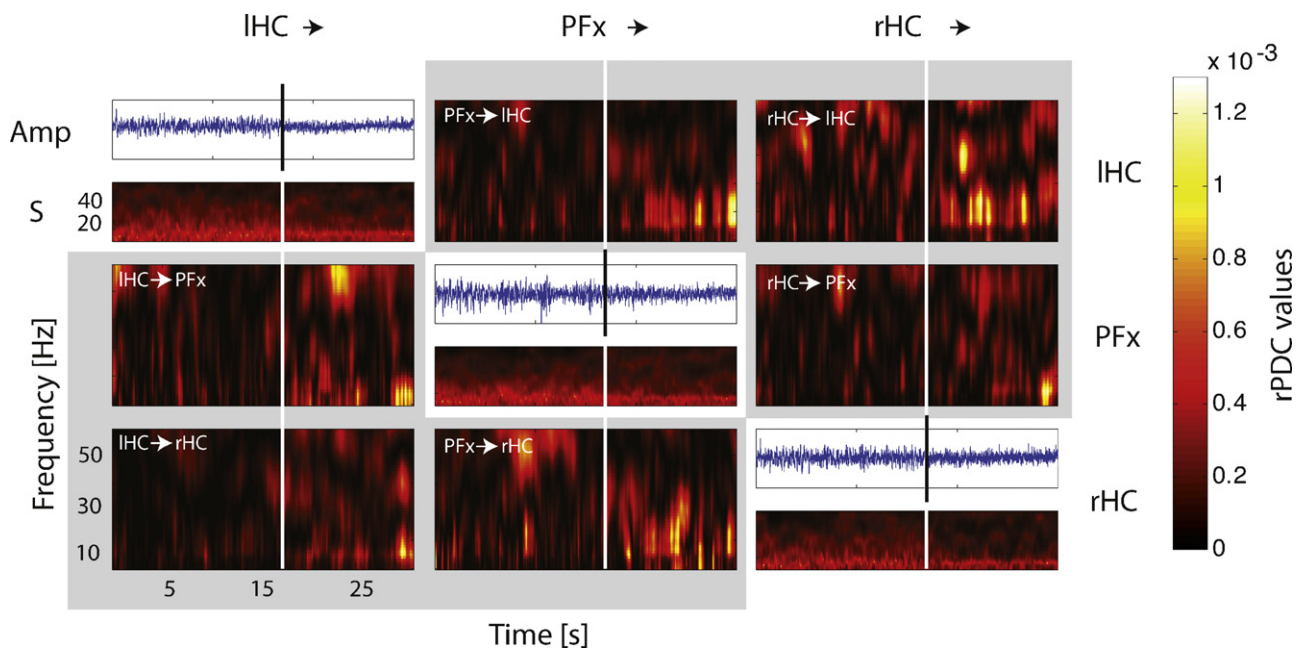


**Fig. 9.** Renormalized partial directed coherence analysis applied to murine EEG data recorded bilaterally above the hippocampus (left: IHC, right: rHC), and prefrontal cortex (Pfx). Raw data are depicted on the diagonal (amplitude (Amp) in arbitrary units) over time in seconds, presented together with the autospectra (S) – logarithm of the spectra color coded with respect to frequency in Hz (y-axis) and time in samples (x-axis). The lines indicate the time point of transition between NREM to REM sleep, the gray underlay denotes the time resolved rPDC analysis – direction of information flow is from column to row. Color coding indicates intensity of coherence.

stages, which may ultimately allow the identification of transition-specific patterns.

## 7. Conclusion

Detection of relationships and causal influences are of particular interest in multivariate time series analysis. This is commonly hampered by time-dependent dynamics and especially relationships between processes. Moreover, time series generated by underlying stochastic processes are contaminated with observational noise. We presented a new approach to address both challenges. Combination of renormalized partial directed coherence and state space models is feasible to detect time variant causal influences in noisy multivariate processes. It allows to detect transitions for example from slow-wave to REM sleep and thus offers a more detailed insight into the dynamics of the brain.

Further studies should also include non-linear processes. For non-linear systems, a higher order of the VAR process may also yield information about causal, time-dependent influences. Using state space modeling alone often leads to hardly interpretable results, if too many parameters are unequal to zero. This difficulty is overcome by renormalized partial directed coherence. Since, the latter is estimated in the frequency domain, it allows detecting causal influences at frequencies that are of interest (e.g. theta range in REM sleep), advantageous for oscillatory processes in applications like EEG analysis. Furthermore, a time-dependency in the parameter estimation is intrinsic to the analysis. This is superior to epoch-based data analysis since only piece-wise constant parameters can be detected in this way. Moreover, the epoch duration would have to be pre-selected. Since some vigilance stages such as REM sleep can be very short (<10 s), equivalent epochs would have to be chosen. The length of the epochs restricts the maximum order that can be used for autoregressive modeling which in turn restricts the frequency-resolution that can be obtained. Thereby for short epoch only a very low resolution in the frequency-domain is possible. Additionally, cutting points force the parameter estimation technique to assume stationarity for each epoch, introducing a potential dependence on the choice of cut points.

Another successful approach dealing with time and frequency resolution of data are wavelets (Dhamala et al., 2008; Sato et al., 2006). In future, wavelet based techniques should be compared to the method presented here. Thereby, revealing the advantages of both approaches and possibly a way to combine them.

The combination and enhancement of renormalized partial directed coherence and state space modeling with extended Kalman filtering allows for detection of time-dependent and eventually continuously changing causal influences in multivariate

linear processes. Future applications could include ageing, sleep studies as well as nervous system diseases. The code is available upon request from the authors.

## Acknowledgments

The authors like to thank Johannes Wohlmuth for many fruitful discussions, calculations and the contributions to the code. This work was supported by the German Science Foundation (Ti315/4-2), the German Federal Ministry of Education and Research (BMBF Grant O1GQ0420), and the Excellence Initiative of the German Federal and State Governments. B.S. and L.S. are indebted to the Landesstiftung Baden-Württemberg for the financial support of this research project by the Eliteprogramme for Postdocs. This work was partially funded by the UK Biotechnology and Biological Sciences Research Council under the Systems Approaches to Biological Research (SABR) Initiative (BB/FO0513X/1).

## Appendix A. Improvement of the dual Kalman filter

For brevity we define  $\mathbf{C}_{t,a} := \tilde{\mathbf{C}}_a^{t-1|t-1}$  and  $\mathbf{A}_{t|t-1} := \tilde{\mathbf{A}}^{t-1|t-1}$ . The random vector  $\tilde{\mathbf{a}}(t-1)$  originates from the process state Eq. (24)

$$\tilde{\mathbf{u}}(t) = \mathbf{A}^{\tilde{\mathbf{a}}(t-1)} \tilde{\mathbf{u}}(t-1) + \tilde{\boldsymbol{\epsilon}}_u(t), \quad (\text{A.1})$$

where the dependences of  $\mathbf{A}$  on the parameter state variable  $\tilde{\mathbf{a}}(t-1)$  are highlighted in red. Instead of replacing the random variable  $\tilde{\mathbf{a}}(t-1)$  in the process state space by its estimator  $\tilde{\mathbf{a}}(t-1|t-1)$ , as the standard dual Kalman filter does,  $\tilde{\mathbf{a}}(t-1)$  is treated as a random variable and (A.1) as a nonlinear equation that is approximated by a Taylor expansion of first order around  $\tilde{\mathbf{u}}(t-1)$  and  $\tilde{\mathbf{a}}(t-1)$ . In the extended Kalman filter the prediction of the variance  $\mathbf{P}_{t|t-1}^z$  is approximated in the same way by the first order Taylor expansion of  $\tilde{\mathbf{z}}(t) = f(\tilde{\mathbf{z}}(t-1)) + \tilde{\boldsymbol{\epsilon}}_z(t)$  around  $\tilde{\mathbf{z}}(t-1) = (\tilde{\mathbf{a}}^T(t-1), \tilde{\mathbf{u}}^T(t-1))^T$ . Therefore, the prediction of the variance of the joint state space  $\mathbf{P}_{t|t-1}^z$  is estimated based on the variance matrix  $\mathbf{P}_{t-1|t-1}^z$ . The latter contains the same information as the dual Kalman filter, i.e.  $\mathbf{P}_{t-1|t-1}^z$  has block diagonal form with  $\mathbf{P}_{t-1|t-1}^a$  and  $\mathbf{P}_{t-1|t-1}^u$  on its diagonal. The result of the predicted submatrix  $\mathbf{P}_{t|t-1}^u$  of  $\mathbf{P}_{t-1|t-1}^z$  leads to the improved variance matrix of the process state space. For the derivation, the process state  $\tilde{\mathbf{u}}(t) = (\tilde{\mathbf{x}}^T(t), \tilde{\mathbf{x}}^T(t-1), \dots, \tilde{\mathbf{x}}^T(t-p+1))^T$  is divided into the actual process state vector  $\tilde{\mathbf{x}}(t)$  and the past of the process state vector  $\tilde{\mathbf{x}}^{\text{past}}(t) = (\tilde{\mathbf{x}}^T(t-1), \dots, \tilde{\mathbf{x}}^T(t-p+1))^T$ . In the same way, the transition matrix  $\mathbf{A}_{t|t-1}$  of the process state space is divided into the first  $n$  rows  $\mathbf{A}_{t|t-1}^0$  containing all parameters  $\tilde{\mathbf{a}}(t-1|t-1)$  and  $\mathbf{A}^1$  with the remaining  $(p-1)n$  constant rows. The prediction of the variance of the joint state vector

$$\begin{aligned} \mathbf{P}_{t|t-1}^z &= \mathbf{J}_t \mathbf{P}_{t-1|t-1}^z \mathbf{J}_t^T + \mathbf{Q}^z \\ &= \left( \begin{array}{c|c} \mathbf{I}_{n_a} & \mathbf{0}_{n_a \times n_x} \\ \mathbf{C}_{t,a} & \mathcal{A}_t^0 \\ \mathbf{0}_{(n_x-n) \times n_a} & \mathcal{A}^1 \end{array} \right) \left( \begin{array}{c|c} \mathbf{P}_{t-1|t-1}^a & \mathbf{0}_{n_a \times n_x} \\ \mathbf{0}_{n_x \times n_a} & \mathbf{P}_{t-1|t-1}^u \end{array} \right) \\ &\quad \cdot \left( \begin{array}{c|c} \mathbf{I}_{n_a} & \mathbf{C}_{t,a}^T \\ \mathbf{0}_{n_x \times n_a} & (\mathcal{A}_t^0)^T \end{array} \right) + \left( \begin{array}{c|c} \mathbf{Q}_a & \mathbf{0} \\ \mathbf{0} & \Sigma \\ \mathbf{0} & \mathbf{0} \end{array} \right) \\ &= \left( \begin{array}{c|c|c} \mathbf{P}_{t-1|t-1}^a + \mathbf{Q}_a & \mathbf{P}_{t-1|t-1}^a \mathbf{C}_{t,a}^T & \mathbf{0}_{n_a \times (n_x-n)} \\ \mathbf{C}_{t,a} \mathbf{P}_{t-1|t-1}^a & \mathcal{A}_{t|t-1}^0 \mathbf{P}_{t-1|t-1}^u (\mathcal{A}_{t|t-1}^0)^T + \mathbf{C}_{t,a} \mathbf{P}_{t-1|t-1}^a \mathbf{C}_{t,a}^T + \Sigma & \mathcal{A}_{t|t-1}^0 \mathbf{P}_{t-1|t-1}^u (\mathcal{A}^1)^T \\ \mathbf{0}_{(n_x-n) \times n_a} & \mathcal{A}^1 \mathbf{P}_{t-1|t-1}^u (\mathcal{A}_{t|t-1}^0)^T & \mathcal{A}^1 \mathbf{P}_{t-1|t-1}^u (\mathcal{A}^1)^T \end{array} \right) \\ &= \left( \begin{array}{c|c|c} \mathbf{P}_{t|t-1}^a & \mathbf{P}_{t|t-1}^{ax} & \mathbf{0} \\ \mathbf{P}_{t|t-1}^{xa} & \mathbf{P}_{t|t-1}^x & \mathbf{P}_{t|t-1}^{xx \text{ past}} \\ \mathbf{0} & \mathbf{P}_{t|t-1}^{x \text{ past}} & \mathbf{P}_{t|t-1}^x \end{array} \right). \end{aligned} \quad (\text{A.2})$$

is using the same information as the dual Kalman filter. The differences between the variance predictions of the standard dual Kalman filter  $\mathbf{P}_{t|t-1}^a$  and  $\mathbf{P}_{t|t-1}^u$  and the extended Kalman filter are highlighted in red. The changes in  $\mathbf{P}_{t|t-1}^u$  are used to improve the prediction of the variance of the dual Kalman filter. The first  $n$  components  $\bar{x}(t)$  of the process state vector  $\bar{u}(t)$  are predicted through the transition matrix  $\mathbf{A}_t^0$  incorporating the parameter vector  $\bar{a}(t)$ . The result for the variance of the actual process state vector in (A.2)

$$\mathbf{P}_{t|t-1}^x = \mathbf{A}_{t|t-1}^0 \mathbf{P}_{t-1|t-1}^u (\mathbf{A}_{t|t-1}^0)^T + \mathbf{C}_{t,a} \mathbf{P}_{t-1|t-1}^a \mathbf{C}_{t,a}^T + \Sigma \quad (\text{A.3})$$

treats the parameters  $\bar{a}(t)$  as a random vector and incorporates its variance into the prediction of the variance  $\mathbf{P}_{t|t-1}^x$ . This corresponds to a multivariate Gaussian error propagation. The correlations  $\mathbf{P}_{t|t-1}^{ax} = \mathbf{P}_{t-1|t-1}^a \mathbf{C}_{t,a}^T$  are not considered in the dual Kalman filter, but they show that the nonlinear model correlates the parameter and process vectors.

## Appendix B. Methods to speed-up the algorithm

The state space representation of an  $n$ -dimensional VAR[ $p$ ] process requires a  $n_u = np$ -dimensional process state vector while the parameter space is  $n_a = n^2 p$ -dimensional. The joint state space is always  $n_z = n_u + n_a$ -dimensional. The matrix inversion of  $\mathbf{P}_{t|t-1}^a$ , performed in every step of the smoothing filter, requires 80% of the entire computing time. Thus, we present an alternative smoothing algorithm for linear state spaces. This so-called disturbance smoother

$$\bar{\eta}_{t|N} = \mathbf{R}_t [(\mathbf{P}_{t|t-1}^y)^{-1} (\bar{y}_t - \bar{y}_{t|t-1}) - \mathbf{K}_t^T \mathbf{A}_{t+1}^T \bar{r}_t] \quad (\text{B.1})$$

$$\mathbf{P}_{t|N}^y = \mathbf{R}_t - \mathbf{R}_t [(\mathbf{P}_{t|t-1}^y)^{-1} + \mathbf{K}_t^T \mathbf{A}_{t+1}^T \mathbf{F}_t \mathbf{A}_{t+1} \mathbf{K}_t] \quad (\text{B.2})$$

$$\bar{\epsilon}_{t|N} = \mathbf{Q}_t \bar{r}_t \quad (\text{B.3})$$

$$\mathbf{P}_{t|N}^\epsilon = \mathbf{Q}_t - \mathbf{Q}_t \mathbf{F}_t \mathbf{Q}_t \quad (\text{B.4})$$

$$\mathbf{F}_{t-1} = \mathbf{C}_t^T (\mathbf{P}_{t|t-1}^y)^{-1} \mathbf{C}_t + \mathbf{E}_t^T \mathbf{F}_t \mathbf{E}_t \quad (\text{B.5})$$

$$\bar{r}_{t-1} = \mathbf{C}_t^T (\mathbf{P}_{t|t-1}^y)^{-1} (\bar{y}_t - \bar{y}_{t|t-1}) + \mathbf{E}_t^T \bar{r}_t \quad (\text{B.6})$$

$$\mathbf{E}_t = \mathbf{A}_{t+1} (\mathbf{I}_{n_u} - \mathbf{K}_t \mathbf{C}_t) \quad (\text{B.7})$$

is derived in detail in Durbin and Koopman (2001). Based on this, the estimators for the hyper-parameters

$$\mathbf{R}^{(m+1)} = \frac{1}{N} \sum_{t=1}^N \{ \bar{\eta}_{t|N} \bar{\eta}_{t|N}^T + \mathbf{P}_{t|N}^y \} \quad (\text{B.8})$$

$$\mathbf{Q}^{(m+1)} = \frac{1}{N} \sum_{t=1}^N \{ \bar{\epsilon}_{t|N} \bar{\epsilon}_{t|N}^T + \mathbf{P}_{t|N}^\epsilon \} \quad (\text{B.9})$$

in the  $m$ th expectation–maximization iteration are derived. Applying the disturbance smoother to dual state space representation of the time-dependent  $n$ -dimensional VAR[ $p$ ] process, only the inverse of the  $n \times n$  matrices  $\mathbf{P}_{t|t-1}^y$  and  $\mathbf{P}_{t|t-1}^a$  are required and the computationally expensive inversion of the  $n_u \times n_u$  matrix  $\mathbf{P}_{t|t-1}^u$  and the  $n_a \times n_a$  matrix  $\mathbf{P}_{t|t-1}^a$  drop out. This leads to an increased speed of about 20–30%.

The dual Kalman filter successfully reduced the computing time by separating the  $n_z = n_u + n_a$ -dimensional joint state space into two state spaces with dimensions  $n_u$  and  $n_a$ . In the same way, the parameter state space  $\bar{a}_t = (\bar{a}_{1,t} \dots \bar{a}_{n,t})$  can be separated into  $n$  parameter sub-state spaces  $\bar{a}_{j,t}$ . Thus, the sub-state spaces are only  $n_u$ -dimensional reducing the computing time and memory storage. The separated parameter state space models cannot consider the correlations between  $\bar{a}_{j,t}$  and  $\bar{a}_{k,t}$  for  $k \neq j$ . Additionally

the different components  $x_{j,t}$  may not be mixed in the observation equation, i.e. the observation matrix  $\mathbf{C}_x$  must be diagonal. Knowing the constraints of this representation, the Kalman filter can be applied.

## References

- Akaike H. A new look at the statistical model identification. *IEEE Trans Automat Contr* 1974;19:716–23.
- Andrzejak RG, Ledberg A, Deco G. Detecting event-related time-dependent directional couplings. *New J Phys* 2006;8:6.
- Ansley CF, Kohn R. A geometrical derivation of the fixed interval smoothing algorithm. *Biometrika* 1982;69:486–7.
- Arnhold J, Grassberger P, Lehnertz K, Elger CE. A robust method for detecting interdependencies: application to intracranially recorded EEG. *Physica D* 1999;134:419–30.
- Arnold M, Miltner WHR, Witte H, Bauer R, Braun C. Adaptive AR modeling of non-stationary time series by means of Kalman filtering. *IEEE Trans Biomed Eng* 1998;45:553–62.
- Baccala LA, Sameshima K. Directed coherence: a tool for exploring functional interactions among brain structures. In: Nicolelis MAL, editor. *Methods for neural ensemble recordings*. Boca Raton; 1998. p. 179–92.
- Baccala LA, Sameshima K. Partial directed coherence: a new concept in neural structure determination. *Biol Cybern* 2001;84:463–74.
- Baccala LA, Sameshima K, Ballester G, Valle AC, Timo-Jaria C. Studying the interaction between brain structures via directed coherence and Granger causality. *Appl Signal Process* 1998;5:40–8.
- Bahraminasab A, Ghasemi F, Stefanovska A, McClintock PVE, Friedrich R. Physics of brain dynamics: Fokker–Planck analysis reveals changes in EEG  $\delta$ – $\theta$  interactions in anesthesia. *New J Phys* 2009;11:103051.
- Brillinger D. *Time series: data analysis and theory*. Holden-Day; 1981.
- Brockwell PJ, Davis RA. *Time series: theory and methods*. Springer-Verlag; 1993.
- Brovelli A, Ding M, Ledberg A, Chen Y, Nakamura R, Bressler SL. Beta oscillations in a large-scale sensorimotor cortical network: directional influences revealed by granger causality. *Proc Natl Acad Sci USA* 2004;101(June):9849–54.
- Chicharro D, Andrzejak RG. Reliable detection of directional couplings using rank statistics. *Phys Rev E* 2009;80:026217.
- Dahlhaus R. Graphical interaction models for multivariate time series. *Metrika* 2000;51:157–72.
- Dahlhaus R, Eichler M. Causality and graphical models in time series analysis. In: Green P, Hjort N, Richardson S, editors. *Highly structured stochastic systems*. Oxford statistical science series, vol. 27. Oxford University Press; 2003. p. 115–37.
- Dempster A, Laird N, Rubin D. Maximum likelihood from incomplete data via the EM algorithm. *J Roy Stat Soc, Ser B* 1977;39:1–38.
- Dhamala M, Rangarajan G, Ding M. Estimating Granger causality from Fourier and wavelet transforms of time series data. *Phys Rev Lett* 2008;100:018701.
- Durbin J, Koopman SJ. *Time series analysis by state space methods*. Oxford statistical science series, vol. 24. Oxford University Press; 2001.
- Eichler M. Granger-causality graphs for multivariate time series. University of Heidelberg; 2000. Preprint.
- Frenzel S, Pompe B. Partial mutual information for coupling analysis of multivariate time series. *Phys Rev Lett* 2007;99:204101.
- Gluckman B, Nguyen H, Weinstein S, Schiff S. Adaptive electric field control of epileptic seizures. *J Neurosci* 2001;21:590–600.
- Grenier Y. Time-dependent ARMA modeling of nonstationary signals. *IEEE Trans Acoust Signal Process* 1983;31:899–911.
- Halliday DM, Rosenberg JR. On the application, estimation and interpretation of coherence and pooled coherence. *J Neurosci Methods* 2000;100:173–4.
- Hamilton JD. *Time series analysis*. Princeton University Press; 1994.
- Harvey AC. *Forecasting, structural time series models and the Kalman filter*. Cambridge University Press; 1994.
- Hemmelmann D, Ungureanu M, Hesse W, Wüstenberg T, Reichenbach JR, Witte OW, et al. Modelling and analysis of time-variant directed interrelations between brain regions based on BOLD-signals. *Neuroimage* 2009;45:722–37.
- Honerkamp J. *Stochastic dynamical systems*. Wiley-VCH; 1993.
- Horwitz B. The elusive concept of brain connectivity. *Neuroimage* 2003;19:466–70.
- Julier S, Uhlmann F, Durrant-Whyte HF. A new method for the nonlinear transformation of means and covariances in filters and estimators. *IEEE Trans Autom Control* 2000;45:477–82.
- Jyoti A, Plano A, Riedel G, Platt B. EEG, activity, and sleep architecture in a transgenic  $\alpha$ ppsw/psen1a246e Alzheimer's disease mouse. *J Alzheimers Dis* 2010;22:873–87.
- Kalman RE. A new approach to linear filtering and prediction problems. *Trans ASME, J Basic Eng* 1960;82:35–45.
- Kalman RE, Bucy RS. New results in linear filtering and prediction theory. *Trans ASME, J Basic Eng* 1961;83:95–107.
- Kamiński MJ, Blinowska KJ. A new method of the description of the information flow in the brain structures. *Biol Cybern* 1991;65:203–10.
- Kamiński MJ, Blinowska KJ, Szelenberger W. Topographic analysis of coherence and propagation of EEG activity during sleep and wakefulness. *Electroenceph Clin Neurophys* 1997;102:216–27.
- Kitagawa G, Gersch W. *Smoothness priors analysis of time series*. Lecture notes in statistics, vol. 116. New York: Springer-Verlag; 1996.

- Korzeniewska A, Kasicki S, Kamiński MJ, Blinowska KJ. Information flow between hippocampus and related structures during various types of rat's behavior. *J Neurosci Methods* 1997;73:49–60.
- Lawrie SM, Buechel C, Whalley HC, Frith CD, Johnstone EC. Reduced frontotemporal functional connectivity in schizophrenia associated with auditory hallucinations. *Biol Psychiatry* 2002;51(June):1008–11.
- Lütkepohl H. Introduction to multiple time series analysis. Springer-Verlag; 1993.
- Martini M, Kranz TA, Wagner T, Lehnertz T. Inferring directional interactions from transient signals with symbolic transfer entropy. *Phys Rev E* 2011;83:011919.
- Nicolelis MAL, Fanselow EE. Thalamocortical optimization of tactile processing according to behavioral state. *Nat Neurosci* 2002;5:517–23.
- Nolte G, Ziehe A, Nikulin VV, Schlögl A, Krämer N, Brismar T, et al. Robustly estimating the flow direction of information in complex physical systems. *Phys Rev Lett* 2008;100:234101.
- Paluš M, Stefanovska A. Direction of coupling from phases of interacting oscillators: an information-theoretic approach. *Phys Rev E* 2003;67:055201(R).
- Paluš M, Vejmelka M. Directionality of coupling from bivariate time series: how to avoid false causalities and missed connections. *Phys Rev E* 2007;75:056211.
- Pompe B, Blidh P, Hoyer D, Eiselt M. Using mutual information to measure coupling in the cardiorespiratory system. *IEEE Eng Med Biol* 1998;17:32–9.
- Prussek J, Lehnertz K. Measuring interdependences in dissipative dynamical systems with estimated Fokker-Planck coefficients. *Phys Rev E* 2008;77:041914.
- Rauch HE, Tung F, Striebel CR. Maximum Likelihood estimates of linear dynamic systems. *AIAA J* 1965;3:1445–50.
- Romano MC, Thiel M, Kurths J, Grebogi C. Estimation of the direction of the coupling by conditional probabilities of recurrence. *Phys Rev E* 2007;76:036211.
- Rosenblum MG, Cimponeriu L, Bezerianos A, Patzak A, Mrowka R. Identification of coupling direction: application to cardiorespiratory interaction. *Phys Rev E* 2002;65:041909.
- Rosenblum MG, Pikovsky AS. Detecting direction of coupling in interacting oscillators. *Phys Rev E* 2001;64:045202.
- Sameshima K, Baccala LA. Using partial directed coherence to describe neuronal ensemble interactions. *J Neurosci Methods* 1999;94:93–103.
- Sato JR, Junior EA, Takahashi DY, de Maria Felix M, Brammer MJ, Morettn PA. A method to produce evolving functional connectivity maps during the course of an fMRI experiment using wavelet-based time-varying Granger causality. *Neuroimage* 2006;31:187–96.
- Schack B, Griebach G, Arnold M, Bolten J. Dynamic cross-spectral analysis of biological signals by means of bivariate ARMA processes with time-dependent coefficients. *Med Biol Eng Comput* 1995;33:605–10.
- Schelter B, Timmer J, Eichler M. Assessing the strength of directed influences among neural signals using renormalized partial directed coherence. *J Neurosci Methods* 2009;179:121–30.
- Schreiber T. Measuring information transfer. *Phys Rev Lett* 2000;85:461–4.
- Schwarz G. Estimating the dimension of a model. *Ann Stat* 1978;6:461–4.
- Seth AK, Edelman GM. Distinguishing causal interactions in neural populations. *Neural Comput* 2007;19:910–33.
- Shumway RH, Stoffer DS. An approach to time series smoothing and forecasting using the EM algorithm. *J Time Ser Anal* 1982;3:253–64.
- Shumway RH, Stoffer DS. Time series analysis and its applications. New York: Springer; 2000.
- Sommerlade L, Eichler M, Jachan M, Henschel K, Timmer J, Schelter B. Estimating causal dependencies in networks of nonlinear stochastic dynamical systems. *Phys Rev E* 2009;80:051128.
- Staniek M, Lehnertz K. Symbolic transfer entropy. *Phys Rev Lett* 2008;100:158101.
- Sunderam S, Chernyy N, Peixoto N, Mason JP, Weinstein SL, Schiff SJ, et al. Improved sleep-wake and behavior discrimination using mems accelerometers. *J Neurosci Methods* 2007;163:373–83.
- Sunderam S, Gluckman B, Reato D, Bikson M. Toward rational design of electrical stimulation strategies for epilepsy control. *Epilepsy Behav* 2010;17:6–22.
- Timmer J. Modeling noisy time series: physiological tremor. *Int J Bifurcation Chaos* 1998;8:1505–16.
- Vejmelka M, Paluš M. Inferring the directionality of coupling with conditional mutual information. *Phys Rev E* 2008;77:026214.
- Wagner T, Fell J, Lehnertz K. The detection of transient directional couplings based on phase synchronization. *New J Phys* 2010;12:053031.
- Wan EA, Nelson AT. Neural dual extended Kalman filtering: applications in speech enhancement and monaural blind signal separation. *IEEE Proc Neural Netw Signal Process* 1997:466–75.
- Wan EA, van der Merwe R. The unscented Kalman filter for nonlinear estimation. *IEEE Commun Contr Symp Adapt Syst Signal Process* 2000:152–8.
- Winterhalder M, Schelter B, Hesse W, Schwab K, Leistriz L, Klan D, et al. Comparison of linear signal processing techniques to infer directed interactions in multivariate neural systems. *Sig Proc* 2005;85:2137–60.